Geometric interpretation of four-wave mixing

J. R. Ott,[1,2,*] H. Steffensen,[1] K. Rottwitt,[1,†] and C. J. McKinstrie[3,‡]

[1]*Department of Photonics Engineering Fotonik-DTU, Technical University of Denmark, DK-2800 Kongens Lyngby, Denmark*

[2]*Départment de Physique Théorique, Universite de Genève, CH-1202 Genève, Switzerland*

[3]*Bell Laboratories, Alcatel-Lucent, Holmdel, New Jersey 07733, USA*

(Received 2 July 2013; published 7 October 2013)

The nonlinear phenomenon of four-wave mixing (FWM) is investigated using a method, where, without the need of calculus, both phase and amplitudes of the mixing fields are visualized simultaneously, giving a complete overview of the FWM dynamics. This is done by introducing a set of Stokes-like coordinates of the electric fields, which reduce the FWM dynamics to a closed two-dimensional surface, similar to the Bloch sphere of quantum electrodynamics or the Pointcaré sphere in polarization dynamics. The coordinates are chosen so as to use the gauge invariance symmetries of the FWM equations which also give the conservation of action flux known as the Manley-Rowe relations. This reduces the dynamics of FWM to the one-dimensional intersection between the closed two-dimensional surface and the phase-plane given by the conserved Hamiltonian. The analysis is advantageous for visualizing phase-dependent FWM phenomena which are found in a large variety of nonlinear systems and even in various optical communication schemes.

DOI: 10.1103/PhysRevA.88.043805 PACS number(s): 42.65.Ky, 42.65.Hw, 42.65.Wi

I. INTRODUCTION

Four-wave mixing (FWM) is a third-order nonlinear process arising from the interaction of four waves. This phenomenon is found in many systems ranging from plasma physics [1] to optics [2–4]. In nonlinear optical systems FWM can be intuitively understood by quantum mechanically describing the electric fields. In such a description, two photons of frequencies ω_2 and ω_3 are annihilated while two photons of frequency ω_1 and ω_4 are created (or vice versa) while keeping energy and momentum conserved. These processes can be either nondegenerate, as sketched in Fig. 1, or degenerate (when $\omega_2 = \omega_3$).

The fiber optical parametric process of FWM is currently used for several optical communication schemes such as amplification [5], phase conjugation [6–8], noiseless frequency conversion [9], and pulse regeneration [10,11]. Furthermore, the process shows great prospects in the field of fiber-based quantum information since it offers the possibility of, e.g., single-photon frequency translation [12] and quantum-state-preserving pulse reshaping [13]. These schemes predominantly use two different setups known as phase conjugation (PC), where the two inner bands are stronger than the outer, and Bragg scattering (BS), where one of the inner bands and one of the outer bands are stronger than the two remaining, see Figs. 1(b) and 1(c), respectively. The two setups are governed by the same physics since the power flow from the inner bands to the outer or vice versa and the equations governing FWM and their analytic solutions are well known [2–4,14–16]. The difference between PC and BS though appear in the linearized theory, where they have considerably different solutions and, in quantum mechanical treatments, even different noise properties [9]. The linearized theory though results in incorrect predictions, e.g., of what physical parameters yield optimal power conversion [17,18]. Furthermore, standard linearized and nonlinear solution methods of FWM only give information about the amplitude and relative phase separately. Though in a recent analysis both phase and amplitude were found and visualized in the linearized regime using a coordinate transform to Stokes-like variables [19] following a routine which has previously been used to describe the evolution of polarization [20].

Here we show a simple method, which, without the use of calculus, allows calculating and visualizing simultaneously the field amplitudes *and* relative phase of the full nonlinear problem. The method gives the dynamics as a closed two-dimensional surface in a three -dimensional space, see Fig. 1(d). This is similar to the Poincaré sphere of polarization dynamics or the Bloch sphere of quantum electrodynamics. With the used method the amplitude and phase of the fields are found without having to evaluate any integrals or differential equations, but simply by plotting two implicit equations and observing their intersection. A similar approach has previously been used for three-wave mixing in quadratic nonlinear media [21]. This has been used for optimizing the efficiency and phase of optical parametric amplification in chirped quasi-phase-matched gratings of second-order Nonlinear materials [22–24].

In the following we start by introducing the governing equations for FWM in Sec. II. Furthermore, Sec. II reviews the structure of the Hamiltonian and the use of the Poisson bracket formalism for deriving governing equations. Then in Sec. III we introduce the geometric representation of the FWM equations using Stokes vectors and the Hamiltonian in this new space are found. With this, the evolution in the reduced phase space is investigated in Sec. IV and the known results

*johan.ott@unige.ch
†karo@fotonik.dtu.dk
‡mckinstrie@alcatel-lucent.com

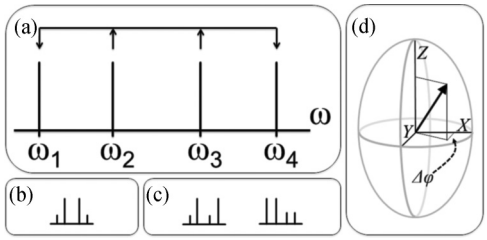

FIG. 1. (a) Sketch of the nondegenerate four-wave mixing process. A photon pair of frequencies ω_2 and ω_3 is annihilated while simultaneously a photon pair at frequencies ω_1 and ω_4 is created (or vice versa). (b,c) show sketches of the phase conjugation and Bragg scattering configurations described in the text. (d) Sketch of the four-wave mixing surface in the Stokes-like variables X, Y, and Z giving the amplitudes of the fields and the phase difference $\Delta\phi$ simultaneously as explained in Sec. III.

are recovered. In Sec. V the geometric representation is used to investigate the PC and BS configurations to visualize the difference between the two. Finally, the paper is concluded in Sec. VI.

II. FOUR-WAVE EQUATIONS AND THEIR SYMMETRIES

In this section the governing equations of FWM are stated and the use of the Poisson bracket formalism to derive the equations of motion along with the Hamiltonian is briefly reviewed. In a normalized form, the well-known governing equations for the nondegenerate FWM process in nonlinear optical fibers are [3,4]

$$\frac{dq_1}{d\xi} = i\Gamma_1 q_1 - i|q_1|^2 q_1 + 2iq_2 q_3 q_4^*, \tag{1a}$$

$$\frac{dq_2}{d\xi} = i\Gamma_2 q_2 - i|q_2|^2 q_2 + 2iq_1 q_3^* q_4, \tag{1b}$$

$$\frac{dq_3}{d\xi} = i\Gamma_3 q_3 - i|q_3|^2 q_3 + 2iq_1 q_2^* q_4, \tag{1c}$$

$$\frac{dq_4}{d\xi} = i\Gamma_4 q_4 - i|q_4|^2 q_4 + 2iq_1^* q_2 q_3. \tag{1d}$$

These are obtained by a slowly varying amplitude approximation of Maxwell's equations for the resonant interaction of four light waves propagating in a centrosymmetric material. The functions q_j are the normalized slowly varying complex field envelopes and the parameters $\Gamma_j = \frac{\beta(\omega_j)}{\gamma_K P}$ are the normalized wave numbers [physical wave number $\beta(\omega_j)$] of the $j = 1,2,3,4$ fields while $\xi = \gamma_K P z$ is the normalized propagation length (physical propagation length z). Both Γ_j's and ξ are normalized with respect to the nonlinear propagation length $\gamma_K P$, where γ_K is the nonlinear Kerr coefficient, for simplicity assumed to be frequency independent, and P is the total action flux. Furthermore, the field envelopes are normalized with respect to P such that

$$|q_1|^2 + |q_2|^2 + |q_3|^2 + |q_4|^2 = 1. \tag{2}$$

The equations have the canonical Hamiltonian structure

$$\frac{dq_j}{dz} = i\frac{\partial H}{\partial q_j^*}, \tag{3}$$

such that Eqs. (1) are reproduced by applying Eq. (3) to the Hamiltonian

$$H = \sum_{n=1}^{4} \Gamma_n |q_n|^2 - \frac{1}{2}\sum_{n=1}^{4} |q_n|^4 + 2(q_1^* q_2 q_3 q_4^* + q_1 q_2^* q_3^* q_4). \tag{4}$$

In Eq. (4) the first sum corresponds to group velocity dispersion while the second sum concerns the nonlinear phase modulation and the last terms give rise to energy conversion. One can further define the complex Poisson bracket

$$\{P,Q\} = \sum_j \left(\frac{\partial P}{\partial q_j}\frac{\partial Q}{\partial q_j^*} - \frac{\partial P}{\partial q_j^*}\frac{\partial Q}{\partial q_j} \right), \tag{5}$$

such that the equations of motion can be written in a form similar to that of quantum mechanics

$$\frac{dq_j}{d\xi} = i\{q_j, H\}. \tag{6}$$

The complex-valued Poisson bracket formalism is equivalent to the usual real-valued position-momentum formalism described in Ref. [25], but with the use of q_j and q_j^* as the choice of canonical variables. Notice that q_j and q_j^* are independent variables in such complex formalism.

The four-wave equations, Eqs. (1), have certain differential symmetries, namely that they are invariant under the gauge transforms

$$(q_1,q_2,q_3,q_4) \to (q_1 e^{-i\phi_1}, q_2, q_3, q_4 e^{i\phi_1}), \tag{7a}$$

$$(q_1,q_2,q_3,q_4) \to (q_1, q_2 e^{-i\phi_2}, q_3 e^{i\phi_2}, q_4), \tag{7b}$$

$$(q_1,q_2,q_3,q_4) \to (q_1 e^{-i\phi_3}, q_2 e^{-i\phi_3}, q_3, q_4), \tag{7c}$$

$$(q_1,q_2,q_3,q_4) \to (q_1, q_2, q_3 e^{-i\phi_4}, q_4 e^{-i\phi_4}). \tag{7d}$$

From Noether's theorem we know that differential symmetries result in conserved quantities [25] and thus the four-gauge transforms result in the constants of motion

$$K_1 = |q_1|^2 - |q_4|^2, \tag{8a}$$

$$K_2 = |q_2|^2 - |q_3|^2, \tag{8b}$$

$$K_3 = |q_1|^2 + |q_2|^2, \tag{8c}$$

$$K_4 = |q_3|^2 + |q_4|^2, \tag{8d}$$

also known as the Manley-Rowe relations (MRR)s [26,27]. The physical significance of the MRRs can easily be understood by a quantum mechanical interpretation as follows. The first two of the relations signify that in the inner and outer bands photons are created or annihilated in pairs. The third and fourth relations signify that creating the photon pairs in the inner or outer bands annihilates photon pairs in the outer or inner bands. The MRRs are seen to be an overfull set and only three of them are independent. Finally, we notice that the Hamiltonian, Eq. (4), is also a constant of motion.

We end this section by sketching the standard procedure for calculating the FWM dynamics. The Hamiltonian, and thus the governing equations for the fields, is seen only to depend on the phase difference $\Delta\phi = \phi_2 + \phi_3 - \phi_1 - \phi_4$, where the phase is defined by $q_j(\xi) = |q_j(\xi)|e^{i\phi_j(\xi)}$. Because the Hamiltonian only depends on the phase difference, the four complex, corresponding to eight real, coupled nonlinear differential equations governing FWM can be reduced to four equations

governing the real amplitudes $|q_j|$ and one governing equation for the phase difference $\Delta\phi$. Then using three of the conserved quantities, Eqs. (8), these can be reduced to a single potential equation for either of the amplitudes, which is solvable using elliptic integrals. Subsequently all the other amplitudes can be found using the MRRs and the phase difference can be calculated using the conservation of the Hamiltoian [15,16]. In the following the problem is solved in another way without using integrals. This gives a geometric interpretation of all the amplitudes and the phase difference simultaneously.

III. REDUCTION TO FOUR-WAVE SURFACES

In this section the dynamics of the four-wave equations are reduced to dynamics on a closed surface in a three-dimensional space. A simple example of the method is the projection of polarization onto the surface of a sphere. In that case the reduction of dimension is performed by using the Stokes parameters, a set of invariant coordinates with respect to the phase symmetry of the polarization, that project the dynamics onto the Poincaré sphere, see, e.g., Ref. [20]. In our case of FWM, a set of Stokes-like parameters which are invariant under the same gauge transforms, Eqs. (7), must be chosen. Such a set of real parameters X, Y, and Z are

$$X + iY = q_1^* q_2 q_3 q_4^*, \tag{9a}$$

$$Z = \kappa \sum_{n=1}^{4} p_n |q_n|^2, \tag{9b}$$

with $\kappa = (p_1 - p_2 - p_3 + p_4)^{-1}$ and p_n being some constants that can be chosen freely only restrained by $p_1 - p_2 - p_3 + p_4 \neq 0$ corresponding to Z not being a combination of the conserved quantities, Eqs. (8). The choices of the p_n's focus the analysis to specific energy conversions in the FWM dynamics. Three examples of such choices are as follows.

(1) By choosing $p_j = 1$, while $p_{n\neq j} = 0$, Z yield the intensity of the jth field.

(2) Choosing $p_1 = p_4 = 1$ and $p_2 = p_3 = 0$, then Z corresponds to the intensity of the side bands such that Z is maximal when most intensity is in the side bands and minimal when it is in the inner bands. Such a choice would be useful for analyzing optical amplification.

(3) Finally, by choosing $p_1 = -p_2 = 1$ and $p_3 = p_4 = 0$ the value of Z corresponds to the difference between one of the inner bands and one of the side bands. This describe frequency conversion.

The new coordinate Z is connected to either of the field envelopes through $|q_n|^2 = Z - Z_n$ for $n = 1$ and 4 and $|q_n|^2 = Z_n - Z$ for $n = 2$ and 3, where

$$Z_1 = \kappa[p_2 K_3 + p_3(K_1 + K_4) - p_4 K_1], \tag{10a}$$

$$Z_2 = \kappa[p_1 K_3 - p_3 K_2 + p_4(K_2 + K_4)], \tag{10b}$$

$$Z_3 = \kappa[p_1(K_1 + K_4) + p_2 K_2 + p_4 K_4], \tag{10c}$$

$$Z_4 = \kappa[p_1 K_1 + p_2(K_2 + K_4) + p_3 K_4]. \tag{10d}$$

Since the MRRs along with energy conservation are an overcomplete set one can write the Z_n's in terms of only two of the K_n's, e.g., K_1 and K_2. By taking the square modulus of $X + iY$ and expressing the $|q_n|^2$'s in terms of the Z coordinate one obtain the expression

$$\begin{aligned} X^2 + Y^2 &= |q_1|^2|q_2|^2|q_3|^2|q_4|^2 \\ &= (Z - Z_1)(Z - Z_2)(Z - Z_3)(Z - Z_4). \end{aligned} \tag{11}$$

By defining

$$\Xi = X^2 + Y^2 - \prod_n (Z - Z_n), \tag{12}$$

we immediately acquire the implicit equation, $\Xi = 0$, from Eq. (11), which yields a surface in the (X,Y,Z) space. The FWM dynamics is thus restricted to the dynamics on the surface given by $\Xi = 0$. This surface is determined strictly from the definitions of (X,Y,Z) along with the MRRs and not the physical parameters of the system such as group velocity dispersion and nonlinearity and neither the phases of the fields. The surface describes the relative phase of the fields through the X and Y coordinates and the chosen field intensities through Z, specified by the choice of the p_n constants.

To plot the implicit equation $\Xi = 0$ it is necessary to parametrize the coordinates. One way to do this is to write the coordinates as $(X,Y,Z) = (R\cos(\theta), R\sin(\theta), Z)$ then noticing that, from Eq. (12), $\Xi = 0$ implies

$$R^2 = \prod_n (Z - Z_n). \tag{13}$$

Thus, since R is positive, we can write the parametrization as

$$\begin{pmatrix} X \\ Y \\ Z \end{pmatrix} = \begin{pmatrix} \sqrt{\prod_n (Z - Z_n)}\cos(\theta) \\ \sqrt{\prod_n (Z - Z_n)}\sin(\theta) \\ Z \end{pmatrix} \tag{14}$$

with the two parameters $\theta \in [0; 2\pi]$ and $Z \in [Z_{\min}; Z_{\max}]$. Notice that the surface $\Xi = 0$ could equally well be described by a line in the (R,Z) coordinates having only the single parameter Z. The advantage of using a three-dimensional space is the ability to visualize the relative phase of the field envelopes which is given by θ. The minimum and maximum of Z depend on the roots Z_n of the polynomial $\prod_n (Z - Z_n)$ and if choosing $\kappa > 0$ they are given by $Z_{\min} = \max(0, K_1) + Z_1$ and $Z_{\max} = -\max(0, K_2) + Z_2$.

Independent of the choice of p_n's the four-wave surface has three typical shapes shown in Figs. 2(a) to 2(c). The citrus- or rugby-shaped surface shown in Fig. 2(a) occur when $K_1 = K_2 = 0$, which can be seen by noting that $K_1 = K_2 = 0$ implies $K_3 = K_4$ giving (for $\kappa > 0$) $Z_1 = Z_4 = Z_{\min}$ and $Z_2 = Z_3 = Z_{\max}$ such that the top and bottom are double roots of $\prod_n (Z - Z_n)$. A schematic illustration of such a configuration is shown in Fig. 2(d). Similarly, the teardrop shown in Fig. 2(b) occurs when *either* $K_1 = 0$ $K_2 = 0$, as schematically illustrated in Fig. 2(e) for $K_2 = 0$. Finally, the deformed sphere shown in Fig. 2(c) occurs when $K_1 \neq 0$ and $K_2 \neq 0$, see Fig. 2(f). The singular points occur when there is a possibility of a full conversion of energy, either to the inner bands or the side bands which is known only to be possible when either $K_1 = 0$ and/or $K_2 = 0$ and the singularity is a sign that it, in theory, takes infinite propagation to achieve [15].

Using that the Hamiltonian is also a constant of motion, the trajectory for a specific configuration of physical parameters can be found as the intersection between the four-wave surface and the Hamiltonian. The Hamiltonian depends on

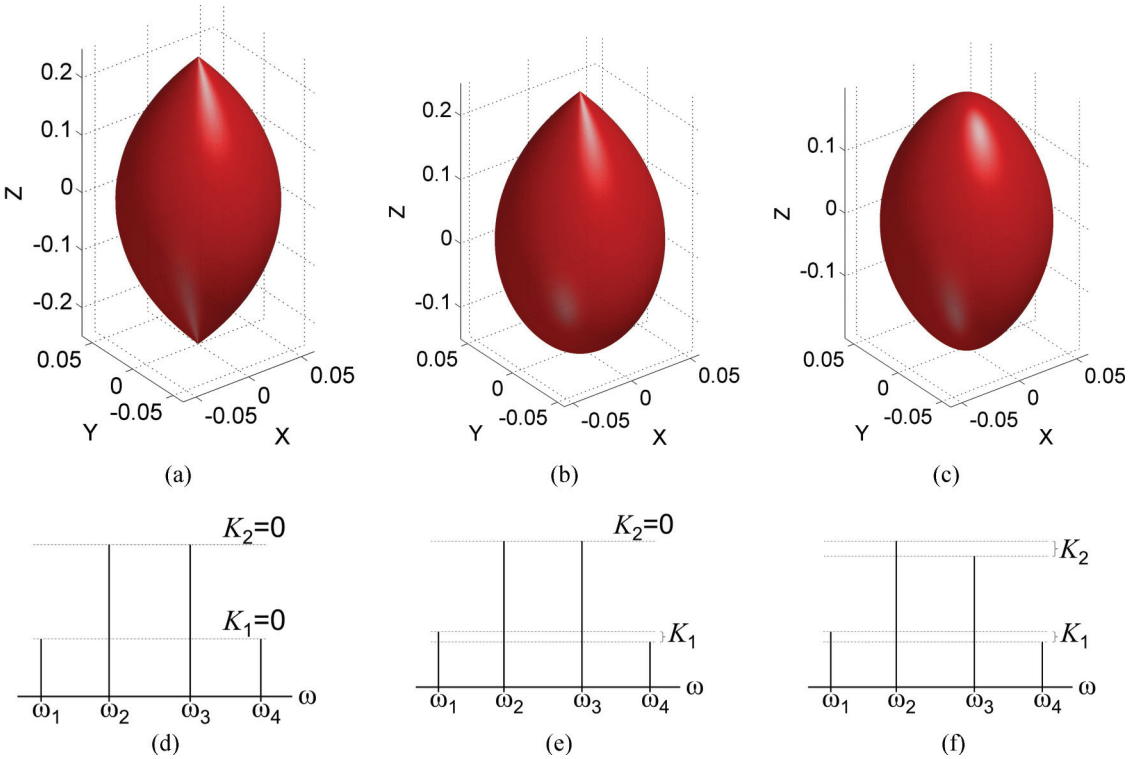

FIG. 2. (Color online) Examples of the FWM surfaces with $p_1 = p_4 = -p_2 = -p_3 = 1$ for different MRRs. The sketches in (d)–(f), respectively, show the configurations which give the surfaces (a)–(c). The specific values of the MRR are (a) $K_1 = K_2 = 0$, $K_3 = K_4 = 0.5$; (e) $K_1 = 0.2$, $K_2 = 0$, $K_3 = 0.6$, and $K_4 = 0.4$,; and (f) $K_1 = K_2 = 0.1$, $K_3 = 0.6$, and $K_4 = 0.4$.

the dispersion and the phase of the fields, the wave-number mismatch $\Delta\Gamma = \Gamma_1 - \Gamma_2 - \Gamma_3 + \Gamma_4$, the phase mismatch $\Omega = \Delta\Gamma + \sum_n Z_n$, and an unimportant constant which we remove by rescaling. Thereby the Hamiltonian in terms of the (X,Y,Z) coordinates is given by

$$H = -2Z^2 + \Omega Z + 4X, \tag{15}$$

which is noted to be independent of Y, linear in X, and quadratic in Z. Since the Hamiltonian is a constant of motion one has the restriction $H = H_0$ with H_0 being the Hamiltonian for some specific values of (X,Y,Z), e.g., the initial values.

The FWM dynamics is thus also confined by the Hamiltonian being a constant of motion and thus the full dynamics for a given set of initial fields and wave-number mismatch is found by the intersection between the Hamiltonian plane, $H = H_0$ and the FWM surface $\Xi = 0$. Similar to the FWM surface, we need to parametrize the line of intersection to plot it. Again we do this by choosing $(X,Y,Z) = (R\cos(\theta), R\sin(\theta), Z)$, but while only R was restricted by the coordinate Z when dealing with the FWM surface, now also θ is restricted by the conservation of the Hamiltonian $H = H_0$, through

$$\cos(\theta) = \frac{2Z^2 - \Omega Z - 2Z_0^2 + \Omega Z_0 + 4X_0}{4\sqrt{\prod_n (Z - Z_n)}}, \tag{16}$$

where X_0 and Z_0 are the initial values of X and Z. The observant reader may notice the similarities between the method described here and using the the conservation of the Hamiltonian to plot the FWM dynamics in a phase plane as described in Refs. [16,19]. While the phase plane is a simple way to predict the FWM dynamics from the knowledge of the Hamiltonian it is limited to show the prediction for a specific set of physical parameters (here $\Delta\Gamma$) at a time. The method presented here, on the contrary, is able to show the predictions of multiple sets of physical parameters simultaneously.

IV. REDUCED PHASE-SPACE EVOLUTION

In this section we derive the dynamic equations for the new coordinates. In the new coordinates the Poisson brackets are given by

$$\{X,Z\} = -iY, \tag{17a}$$
$$\{Y,Z\} = iX, \tag{17b}$$
$$\{Y,X\} = -\frac{i}{2}\frac{\partial \Xi}{\partial Z}. \tag{17c}$$

Using these and the properties of the Poisson bracket

$$\{P,P\} = 0, \tag{18a}$$
$$\{P,Q^2\} = 2Q\{P,Q\}, \tag{18b}$$
$$\{P,Q\} = -\{Q,P\}, \tag{18c}$$

the dynamical equations for the (X,Y,Z) coordinates are

$$\frac{dX}{d\xi} = -4ZY + \Omega Y, \tag{19a}$$
$$\frac{dY}{d\xi} = 4ZX - \Omega X + 2\frac{\partial \Xi}{\partial Z}, \tag{19b}$$
$$\frac{dZ}{d\xi} = -4Y. \tag{19c}$$

In this form the coupling between X and Y, i.e., the evolution of the phase, consist of a contribution equivalent to a harmonic oscillator with frequency $\Omega - 4Z$. This shows that the evolution of the phase is given by both a contribution from linear dispersion Ω and from nonlinear dispersion $-4Z$. Furthermore, Z and Y are coupled nonlinearly through $\partial\Xi/\partial Z$ equivalent to a nonlinear oscillator. The exact evolution can be calculated using the standard potential approach, see the Appendix A.

Let us analyze the linearized equations by assuming that two of the bands are much stronger than the two other. We choose the p_n parameters such that Z corresponds to the weak bands, i.e., the signal and idler bands, and thus ZX, ZY, and Z^n with $n > 1$ are considered small. This gives the linearized equations

$$\frac{dX}{d\xi} \approx \Omega Y, \tag{20a}$$

$$\frac{dY}{d\xi} \approx -\Omega X + BZ + A, \tag{20b}$$

$$\frac{dZ}{d\xi} \approx -4Y, \tag{20c}$$

where, for brevity, we have defined the constants

$$A = 2\sum_{n=1}^{4}\prod_{m\neq n} Z_m, \quad B = -2\sum_{n=1}^{4}\sum_{m\neq n} Z_n Z_m, \tag{21}$$

which depend on the choice of the p_n's and the MRRs.

We now compare the PC and BS configurations. As described in the Introduction for the PC configuration the inner bands are of comparable strength and likewise are the outer bands. In the BS configuration, one of the inner bands and one of the outer bands are of comparable strength and so are the remaining two. With equal weights on the weak bands the PC configuration give, to first order in the weak bands, that $A^{\mathrm{PC}} \approx 0$ and $B^{\mathrm{PC}} \approx -4P_pP_q \approx -1$, where P_p and P_q are the powers of the two strong pumps. Similarly, the BS configuration gives $A^{\mathrm{BS}} \approx 0$ and $B^{\mathrm{BS}} \approx 4P_pP_q \approx 1$. There is thus a subtle difference between the linearized evolution of PC and BS in that BS can be written in the form $\dot{W} = -M \times W$, where $W = (X/\sqrt{P_pP_x}, Y/\sqrt{P_pP_x}, Z)$ and $M = (4\sqrt{P_pP_x}, 0, \Omega)$. The linearized evolution in Stokes space for BS thus corresponds to motion on a spherical surface as is also found in Ref. [19]. On the other hand, the linearized evolution for PC is in general not bounded. This difference can be understood by noting that the BS configuration will be an extreme case of the type sketched in Figs. 2(c) and 2(f) while PC can be of any of the types sketched in Fig. 2 and thus may experience full energy transfer such that the assumption of strong pumps may only be valid initially.

V. EXAMPLES

In the following we use the method to describe two well known setups. First in Sec. V A a parametric amplifier, which corresponds to the PC configuration, and then in Sec. V B frequency conversion which corresponds to the BS configuration.

A. Phase conjugation

Let us analyze a setup where the two inner bands are of comparable strength and similar are the two outer bands, e.g. q_2 and q_3 are the pumps and q_1 and q_4 are known as the signal and idler. We choose $p_1 = p_4 = 1$ such that $Z = Z_{\min}$ signifies that all energy is in the inner bands, q_2 and q_3, while $Z = Z_{\max}$ signifies that all energy is in the outer bands q_1 and q_4. We will consider a case with equal pumps $K_2 = 0$, but unequal sidebands such that $K_1 = 0.2(\neq 0)$. The values of K_1 and K_2 along with the p_n's fully determine the shape of the four-wave surface. The considered scheme describes a two-pump fiber optical parametric amplifier with the possibility of full energy transfer. We investigate the two cases: (i) the case where one of the sidebands (i.e., the idler) is initially zero giving phase insensitive amplification and (ii) the case where none of the fields are initially zero, thereby resulting in phase sensitive amplification.

1. Phase insensitive amplification

We consider the case where the initial amplitudes are $|q_1(0)| = \sqrt{1/5}$, $|q_2(0)| = |q_3(0)| = \sqrt{2/5}$, and $|q_4(0)| = 0$ such that $K_1 = 0.2$ and $K_2 = 0$. The relative phase is unimportant in this case. To determine the evolution on the four-wave surface we only need to calculate the intersection between the Hamiltonian and the four-wave surface. We investigate two cases (1) zero wave-number mismatch $\Delta\Gamma = 0$, which is what is found to be optimal in linear theory [28] and (2) optimal wave-number mismatch for full energy transfer [14]. For zero wave-number mismatch, $\Delta\Gamma = 0$, the Hamiltonian, given by Eq. (15), is shown as the blue parabolic curved plane in Fig. 3. As described in Sec. III the FWM dynamics is then restricted to the intersection between the Hamiltonian and the four-wave surface and is shown as the green solid line. As seen, the zero wave-number mismatch does not reach the top of the teardrop, i.e., it does not yield the full energy transfer as is well known from standard nonlinear analysis [3,4,15,16].

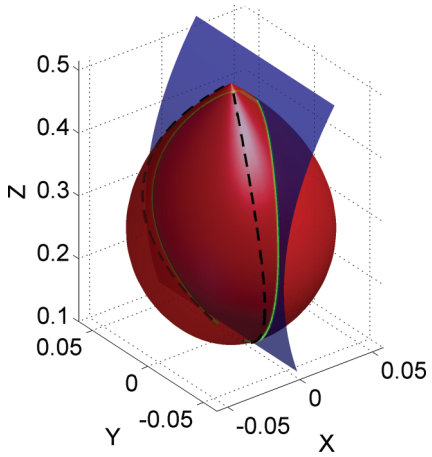

FIG. 3. (Color online) Examples of a phase insensitive PC setup with $\Delta\Gamma = 0$ (paraboloid) and $\Delta\Gamma = \Delta\Gamma_{\mathrm{opt}}$ (dashed line). The specific initial amplitudes are $q_1(0) = \sqrt{1/5}$, $q_2(0) = q_3(0) = \sqrt{2/5}$, and $q_4(0) = 0$. The p_n parameters are $p_1 = p_4 = 1$ and $p_2 = p_3 = 0$ such that the singular point in the top corresponds to full energy transfer from the fields 2 and 3 to 1 and 4.

We now turn to the case of optimal energy transfer. The wave-number mismatch of optimal energy transfer is found by setting $H_0 = H_{\rm opt}$ and isolating $\Delta\Gamma$, where the index 0 denotes the fields at $\xi = 0$ and the index opt denotes the optimal energy transfer. For optimal energy transfer at least one of the fields is fully depleted such that $X_{\rm opt} = 0$ and furthermore $Z_{\rm opt} = Z_{\rm max}$ or $Z_{\rm opt} = Z_{\rm min}$ depending on the choice of p_n's. The resulting wave-number mismatch is thus found from Eq. (15) to be

$$\Delta\Gamma_{\rm opt} = \frac{2\left(Z_{\rm opt}^2 - Z_0^2\right) + 4X_0}{Z_{\rm opt} - Z_0} - \sum_{n=1}^{4} Z_n, \qquad (22)$$

where, expressed in K_1 and K_2, one has $\sum_n Z_n = 1 + 2\kappa K_1(p_1 - p_4) + 2\kappa K_2(p_2 - p_3)$. Notice that the optimal wave-number mismatch depends on X_0 and thus if all the fields have initial nonzero amplitude then $\Delta\Gamma_{\rm opt}$ depends on the initial phase difference of the fields. Such a setup is known as phase sensitive amplification and is discussed in a moment. In the case considered here $p_1 = p_4 = 1$, $p_2 = p_3 = 0$, and $K_2 = 0$ we get $\kappa = \frac{1}{2}$, $X_0 = 0$, $Z_0 = \frac{K_1}{2}$, $Z_{\rm opt} = \frac{1}{2}$, and $\sum_n Z_n = 1$ such that $\Delta\Gamma_{\rm opt} = K_1$. This gives the route for full energy transfer shown in Fig. 3 as the black dashed line.

2. *Phase sensitive amplification*

Before we move on to the BS configuration let us take a look at the phase sensitive amplification scheme, where none of the fields are initially zero. Specifically we consider the initial amplitudes $|q_1(0)| = \sqrt{5/20}$, $|q_2(0)| = |q_3(0)| = \sqrt{7/20}$, and $|q_4(0)| = \sqrt{1/20}$ such that $K_1 = 0.2$ and $K_2 = 0$ thereby giving the same four-wave surface as the above phase insensitive amplification. In this case the relative phase *is* important as is shown in Fig. 4. We choose the wave-number mismatch to be optimal for a relative phase of $\theta = 0$ shown as the black dashed line. By varying the relative phase from 0 to π the Hamiltonian plane is moved towards negative values of X. This can be understood by noting that Z does not change with the phase and thus the change of phase only change X_0 in the Hamiltonian plane being given by $H = H_0$ and thus results in a translation in X. The solid yellow, green, red, and blue lines, respectively, correspondto $\theta = \pi/3$, $\theta = \pi/2$, $\theta = 2\pi/3$, and $\theta = \pi$. It is clear that $\theta = \pi$ yields an amplification which is far from the optimal $\theta = 0$.

B. Bragg scattering

Let us now take a look at a setup where one of the sidebands is comparable in strength with one of the inner bands and similar the remaining bands are of similar strength. This configuration is known as BS and in such a setup both K_1 and K_2 are nonzero. In this case it is impossible to convert all the energy from the pumps to the signal and idler. On the other hand it is always possible to fully convert the energy of the signal onto the idler. We consider a case with fairly strong pumps, specifically the initial amplitudes are $|q_1(0)| = |q_3(0)| = \sqrt{2/100}$ and $|q_2(0)| = |q_4(0)| = \sqrt{48/100}$. Furthermore, we choose $p_1 = -p_3 = 1$ while $p_2 = p_4 = 0$ such that Z is maximal when the total energy of bands 1 and 3 is in band 1 and minimal when it is in band 3. The four-wave surface is shown in Fig. 5 where we have rescaled the X and Y axis with the $|q_2(0)q_4(0)| = (P_2P_4)^{\frac{1}{2}}$ showing how the BS dynamics for strong pumps is restricted to a sphere in the rescaled Stokes space as described in Sec. IV.

For a given $\Delta\Gamma$ we now find the initial relative phase that give a chosen optimal energy conversion. This is done by setting $H_0 = H_{\rm opt}$ and isolating the corresponding relative phase $\theta_0^{\rm opt}$, while noting that Z is phase independent. For optimal conversion $X_{\rm opt} = 0$ and we get from Eq. (15)

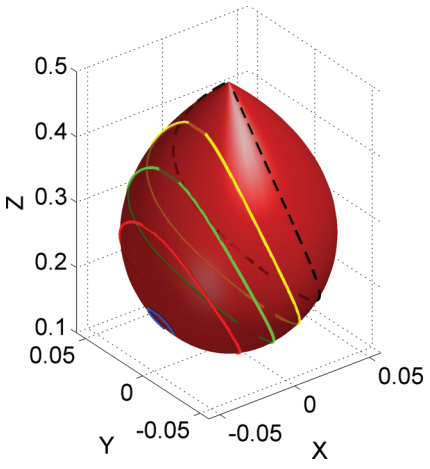

FIG. 4. (Color online) Examples of a phase sensitive PC setup for the specific initial amplitudes $|q_1(0)| = \sqrt{5/20}$, $|q_2(0)| = |q_3(0)| = \sqrt{7/20}$, and $|q_4(0)| = \sqrt{1/20}$, but with the relative phases of $\theta = 0$ (dashed black line), $\theta = \pi/3$ (solid yellow line), $\theta = \pi/2$ (solid green line), $\theta = 2\pi/3$ (solid red line), and $\theta = \pi$ (solid blue line). The wave-number mismatch is chosen for optimal energy transfer for $\theta = 0$. The p_n parameters are $p_1 = p_4 = 1$ and $p_2 = p_3 = 0$ as in Fig. 3.

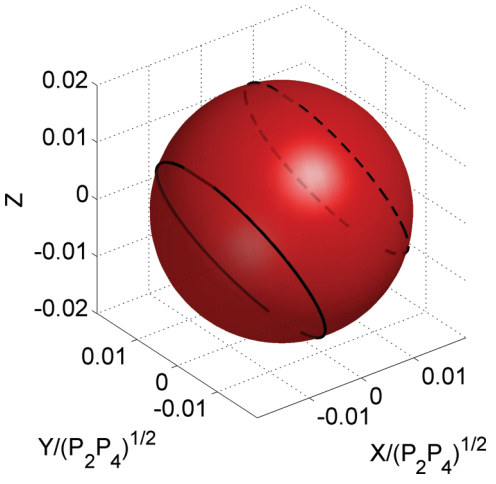

FIG. 5. (Color online) Example of a BS setup for strong pumps. The initial amplitudes are $|q_1(0)| = |q_3(0)| = \sqrt{2/100}$ and $|q_2(0)| = |q_4(0)| = \sqrt{48/100}$. The relative phase θ is chosen using Eq. (23) such that, given a specific $\Delta\Gamma$ (here $= 1$), either energy is transferred to q_1 (dashed black line) or to q_3 (solid black line). The p_n parameters are $p_1 = -p_3 = 1$ and $p_2 = p_4 = 0$ such that $Z_{\rm max}$ corresponds to signal and idler energy being in band 1 while $Z_{\rm min}$ corresponds to the energy being in band 2.

with $X_0 = \sqrt{\prod_n (Z_0 - Z_n)}\cos(\theta_0^{\text{opt}})$

$$\cos\left(\theta_0^{\text{opt}}\right) = \frac{-2\left(Z_{\text{opt}}^2 - Z_0^2\right) + \Omega(Z_{\text{opt}} - Z_0)}{4\sqrt{\prod_n (Z_0 - Z_n)}}. \quad (23)$$

With this we can for a given physical parameter $\Delta\Gamma$, find the optimal relative phase for a preferred frequency conversion. In case we wish to convert all the energy from the bands 1 and 3 into the band 1 we insert $Z_{\text{opt}} = Z_{\max}$ (dashed black line) while if we wish to convert it into band 3 we insert $Z_{\text{opt}} = Z_{\min}$ (solid black line).

VI. CONCLUSION

We have shown a method to visualize the amplitude and phase of FWM processes simultaneously. By defining a set of Stokes-like parameters which are invariant under the same gauge transforms as the traditional FWM equations of motion, the FWM dynamics is reduced to the evolution on a closed surface in the three-dimensional space spanned by the Stokes-like parameters. This four-wave surface is determined solely by the Manley-Rowe relations and is independent of the physical parameters of the nonlinear system. For a given set of physical parameters, i.e., dispersion and Kerr nonlinearity, and initial conditions, i.e., initial wave intensities and phases, the wave dynamics is further restricted by the conservation of the Hamiltonian. The specific evolution of the four-wave dynamics is thus found by the intersection of a parabolic plane spanned by the Hamiltonian and the four-wave surface determined by the Manley-Rowe relations. The method is illustrated in three examples used in optical communications schemes; phase insensitive amplification, phase sensitive amplification, and frequency conversion.

ACKNOWLEDGMENTS

We thank G. G. Luther for valuable discussions. JRO acknowledges financial support from The Danish Council of Independent Research, Natural Sciences.

APPENDIX: STANDARD APPROACH

The evolution of the four-wave equations can of course be solved analytically in the new coordinate system which will be done in the following. In case the p_n's are chosen such that one is unity and the others zero, the analysis reduce to that of Refs. [2,14]. The differentiation of the equation for Z, Eq. (19c), inserting the equation for Y, Eq. (19b), and eliminating X using the conservation of the Hamiltonian such that $H = H_0$, Eq. (15), gives

$$\frac{d^2Z}{d\xi^2} = -f(Z), \quad (A1)$$

where for convenience we have defined

$$f(Z) = -8Z^3 + 6\Omega Z^2 - (4H_0 + \Omega^2)Z + \Omega H_0 - 8\frac{\partial \Xi}{\partial Z}. \quad (A2)$$

Then, by using the mathematical entities that

$$2\frac{dZ}{d\xi}\frac{d^2Z}{d\xi^2} = \frac{d}{d\xi}\left(\frac{dZ}{d\xi}\right)^2 \quad (A3)$$

and that

$$\frac{dZ}{d\xi}f(Z) = \frac{d}{d\xi}\int f(Z)dZ, \quad (A4)$$

the multiplication of Eq. (A1) by $\frac{dZ}{d\xi}$ gives

$$\frac{dZ}{d\xi}\frac{d^2Z}{d\xi^2} = -\frac{dZ}{d\xi}f(Z) = \frac{1}{2}\frac{d}{d\xi}\left(\frac{dZ}{d\xi}\right)^2 = -\frac{d}{d\xi}\int f(Z)dZ. \quad (A5)$$

Thereby, integration gives the potential equation

$$\frac{1}{2}\left(\frac{dZ}{d\xi}\right)^2 + U(Z) = E, \quad (A6)$$

with the potential like function

$$U(Z) = 2Z^4 - 2\Omega Z^3 + 2\left[H_0 + \left(\frac{\Omega}{2}\right)^2\right]Z^2 - \Omega H_0 - 8\Xi(X = Y = 0, Z), \quad (A7)$$

and E is a constant of integration. The potential is a fourth-order polynomial in Z and the potential equation can thus be solved using elliptic functions [29].

The relative phase can then be found from Eq. (16)

$$\cos(\theta) = \frac{2Z^2 - \Omega Z - 2Z_0^2 + \Omega Z_0 + 4X_0}{4\sqrt{\prod_n (Z - Z_n)}}. \quad (A8)$$

[1] R. C. Davidson, *Methods in Nonlinear Plasma Theory* (Academic, New York, 1972).
[2] J. A. Armstrong, N. Bloembergen, J. Ducuing, and P. S. Pershan, Phys. Rev. **127**, 1918 (1962).
[3] R. W. Boyd, *Nonlinear Optics*, 2nd ed. (Academic, San Diego, CA, 2003).
[4] G. Agrawal, *Nonlinear Fiber Optics*, 4th ed. (Academic, San Diego, CA, 2007).
[5] J. Hansryd, P. Andrekson, M. Westlund, J. Li, and P. Hedekvist, IEEE J. Sel. Top. Quantum Electron. **8**, 506 (2002).
[6] A. Yariv, D. Fekete, and D. M. Pepper, Opt. Lett. **4**, 52 (1979).
[7] S. Watanabe and M. Shirasaki, J. Lightwave Technol. **14**, 243 (1996).
[8] C. J. McKinstrie, S. Radic, and C. Xie, Opt. Lett. **28**, 1519 (2003).
[9] C. J. McKinstrie, S. Radic, and M. G. Raymer, Opt. Express **12**, 5037 (2004).
[10] S. Radic, C. J. McKinstrie, R. M. Jopson, J. C. Centanni, and A. R. Chraplyvy, IEEE Photon. Technol. Lett. **15**, 957 (2003).

[11] C. Peucheret, M. Lorenzen, J. Seoane, D. Noordegraaf, C. V. Nielsen, K. Rottwitt, and L. Grüner-Nielsen, IEEE Photon. Technol. Lett. **21**, 872 (2009).
[12] H. J. McGuinness, M. G. Raymer, C. J. McKinstrie, and S. Radic, Phys. Rev. Lett. **105**, 093604 (2010).
[13] C. J. McKinstrie, L. Mejling, M. G. Raymer, and K. Rottwitt, Phys. Rev. A **85**, 053829 (2012).
[14] C. J. McKinstrie and D. F. DuBois, Phys. Rev. Lett. **57**, 2022 (1986).
[15] C. J. McKinstrie and G. G. Luther, Phys. Lett. A **127**, 14 (1988).
[16] G. Cappellini and S. Trillo, J. Opt. Soc. Am. B **8**, 824 (1991).
[17] P. Kylemark, H. Sunnerud, M. Karlsson, and P. A. Andrekson, J. Lightwave Technol. **24**, 3471 (2006).
[18] H. Steffensen, J. R. Ott, K. Rottwitt, and C. J. McKinstrie, Opt. Express **19**, 6648 (2011).
[19] C. J. McKinstrie, Opt. Commun. **282**, 1557 (2009).
[20] J. P. Gordon and H. Kogelnik, Proc. Natl. Acad. Sci. **97**, 4541 (2000).
[21] G. G. Luther, M. S. Alber, J. E. Marsden, and J. M. Robbins, J. Opt. Soc. Am. B **17**, 932 (2000).
[22] C. R. Phillips and M. M. Fejer, Opt. Lett. **35**, 3093 (2010).
[23] C. R. Phillips and M. M. Fejer, Opt. Express **20**, 2466 (2012).
[24] G. Porat and A. Arie, J. Opt. Soc. Am. B **30**, 1342 (2013).
[25] H. Goldstein, *Classical Mechanics*, 2nd ed. (Addison-Wesley, New York, 1980).
[26] J. M. Manley and H. E. Rowe, Proc. IRE **44**, 904 (1956).
[27] M. T. Weiss, Proc. IRE **45**, 1012 (1957).
[28] R. G. Stolen and J. E. Bjorkholm, IEEE J. Quantum Electron. **18**, 1062 (1982).
[29] I. S. Gradshteyn and I. M. Ryzhik, in *Table of Integrals, Series, and Products*, 7th ed., edited by A. Jeffrey and D. Zwillinger, (Academic, San Diego, CA, 2007).